CHAPTER 2.1

ELECTRICAL STIMULATION OF THE PERIPHERAL NERVOUS SYSTEM: BIOPHYSICS AND EXCITATION PROPERTIES

Warren M. Grill
Department of Biomedical Engineering, Case Western Reserve University
Wickenden Bldg. Rm. 139, Cleveland OH 44106-4912
E-mail: wmg@po.cwru.edu

Electrical stimulation of peripheral nerve fibers is an important method to study physiological mechanisms and a technique to restore function to persons with neurological disorders. The processes underlying excitation of nerve fibers are presented through the development of quantitative models of the non-linear properties of the neuronal membrane and the response of nerve fibers to extracellular stimulation. Similarly, the properties of nerve fiber excitation are described and the origins of these properties are explained by reference to the quantitative models. The quantitative treatment of nerve fiber excitation provides the means for understanding the origins of experimentally observed phenomena and a set of tools that can be used to design stimulation paradigms that generate the desired pattern of excitation.

1. Introduction

Electrical activation of the nervous system is used as a tool to study neuroanatomy and neurophysiology, and as a method to restore function to persons following neurological disease or injury. The effects of electrical stimulation on muscular and nervous tissue have been known for over a century, but the underlying biophysical theory to explain these effects was first derived after the development of classical electrodynamics and the development of nerve cell models. We now know that a nerve cell or a nerve fiber can be artificially stimulated (and a propagating action potential generated) by depolarization of the cell's (fiber's) membrane. The propagating action potential reaches the terminal of the axon leading to release of neurotransmitter that can impact the post-synaptic cell or organ. Importantly, whether the action potential was generated naturally or artificially is transparent to the post-synaptic element(s), and this is the basis for neural prostheses[6].

Depolarization can be achieved by a direct outward flowing current injected across the membrane or by generation of a suitable extracellular potential distribution in the vicinity of the cell that indirectly results in an outward flowing transmembrane current and membrane depolarization. Only a suprathreshold current amplitude can generate an

action potential, where the threshold depends on the nerve cell type, its size, the electrode geometry, the electrical properties of the extracellular tissue, and the stimulation parameters.

A distribution of extracellular potentials leading to the generation of an action potential can be generated by electrical current pulses delivered through extracellular electrodes located in the vicinity of the nerve cell bodies or fibers. The electrodes used to deliver the current vary with the site of stimulation and include metal and silicon-based microelectrodes for stimulation of the central nervous system, cuff-type and intraneural wire electrodes for stimulation of peripheral nerves, and intramuscular, epimysial, and skin surface electrodes for stimulation of terminal motor nerve fibers in muscles. The focus of this chapter is on activation of peripheral nerve fibers using either muscle-based or nerve-based electrodes. At this site both sensory and motor nerve fibers can be activated to produce sensations, activate reflex pathways, or create muscular contraction.

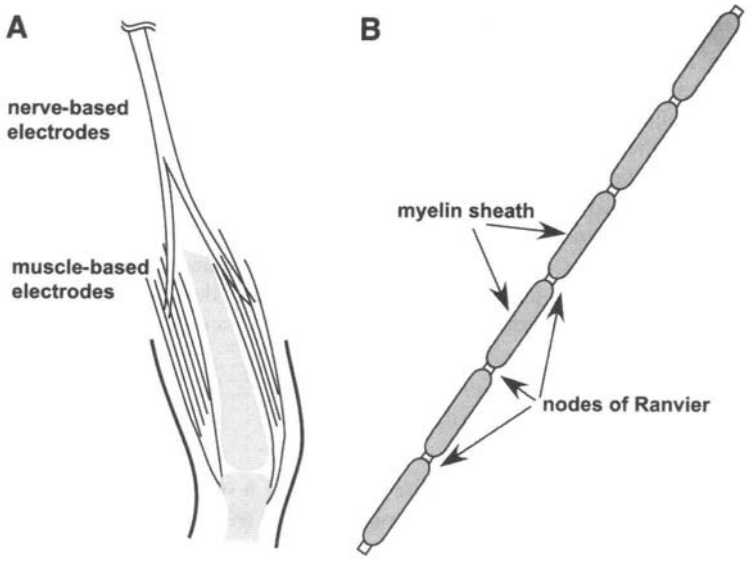

Fig. 1. Electrical stimulation of peripheral nerve fibers. (**A**) Electrodes for stimulation of peripheral nerve fibers may be placed in or on the skeletal muscle (muscle-based electrodes) or in, on, or around the peripheral nerve trunk (nerve-based electrodes). Note that muscle-based electrodes do not activate the muscle directly, but stimulate the terminal nerve fibers that, in turn, activate the muscle. (**B**) The basic structure of a myelinated nerve fiber consists of a tube of membrane, surrounded over most of its area by the myelin sheath. The myelin sheath is interrupted at regular intervals by exposed sections of membrane called nodes of Ranvier.

The objective of this chapter is to present the biophysical basis for electrical stimulation of myelinated axons. The focus will be on electrical stimulation of peripheral myelinated nerve fibers. When considering electrical activation of the nervous system for restoration of motor function, electrodes are most often placed in, on, or around skeletal muscle (muscle-based electrodes, Fig. 1A). Why, if the electrode is placed in or on the

muscle, is the primary concern stimulation of the peripheral nerve? When electrical stimulation is applied to muscle, it is the terminal motor nerve not the muscle that is stimulated. The nerve then releases acetylcholine, which leads, through excitation-contraction coupling, to contraction of the muscle. This was demonstrated by Crago et al.[2] who compared the forces generated by muscle stimulation before and after the application of curare, an agent that blocks neuromuscular transmission. The ratio of force in the blocked preparation to force in the unblocked preparation was ~0.05 demonstrating that the contraction arose from stimulation of the nerve and subsequent activation of the muscle, rather than direct stimulation of the muscle. Further, several limitations of muscle-based electrodes have motivated research on nerve-based electrodes (Fig. 1**A**) that are placed in, on, or around peripheral nerves, and in this location it is clear that it is the nerve that is stimulated.

2. The Peripheral Axon

Peripheral nerve fibers constitute both myelinated nerve fibers and unmyelinated fibers (see Chap. 1.2). In this chapter we focus on excitation of myelinated nerve fibers (Table 1). Myelinated nerve fibers exist in bundles as individual nerve branches or as fascicles within compound peripheral nerve trunks (see Chap. 1.2). Each fiber is essentially a hollow tube of membrane with most of the surface area covered by Schwann cells constituting the myelin (Fig. 1**B**). The myelin sheath is interrupted at regular intervals by exposed portions of membrane called nodes of Ranvier (see Chap. 1.2). The structure of the nerve fiber will form the basis for the models that are subsequently developed, and many of the excitation properties of the nerve fiber (e.g., threshold for excitation, conduction velocity of action potentials) are directly dependent on the morphology of the fiber.

Table 1. Classifications, Functions and Diameters of Peripheral Myelinated Nerve Fibers (see also Chap. 1.2).

Functional Designation	Functional Sub-Type	Actuator/Sensor	Fiber Diameter
A- motor (efferent)	α	Extrafusal muscle fibers	9–20 μm
	β	Extra- and Intra-fusal muscle fibers	9–15 μm
	γ	Intrafusal muscle fibers	2–9 μm
	Iα	Primary Intrafusal Ending	9–22 μm
	Ib	Primary Golgi Tendon Organ Ending	9–22 μm
A- sensory (afferent)	II	Ruffini Endings	5–15 μm
		Secondary Intrafusal Endings	
		Pacinian Corpuscles, Hair Follicles	
	III	Thermoreceptors, Pain Fibers,	1–7 μm
		(free nerve endings?)	
B- preganglionic efferent		Postganglionic neurons	1–3 μm

3. Models of the Axon Membrane

Given the structure of a myelinated nerve fiber, we now go on to develop an electrical circuit model of the nerve fiber (see also Chap. 1.1). We begin by considering a small patch of membrane, as might represent a single node of Ranvier, and then connect these patches to generate a model of the entire axon.

3.1. Passive model of a membrane patch

The lipid bilayer acts as a dielectric between the conductive medium outside the axon and the conductive medium inside the axon (axoplasm). Thus the cell membrane can be modeled as an electrical capacitor (fig. 2A). The thickness of the cell membrane is on the order of 10 nm, and experimental measurements of the capacitance of cell membrane vary from 1–2 $\mu F/cm^2$, yielding a relative dielectric permitivity, ε_r, between 11 and 22, within the range of conventional solid dieletrics ($2 < \varepsilon_r < 100$).

The lack of ionic permeability of the lipid bilayer membrane leads to separation of ionic constituents across the cell membrane. The separation of charged ions gives rise to potential differences (voltages) across the membrane that can be described for each ion using the Nernst Equation, where R is the thermodynamic gas constant, T is the absolute temperature, z is the ionic valency, F is the Faraday constant, and [i] is the concentration of the ion of interest:

$$E_i = \frac{RT}{zF} \log \frac{[i]out}{[i]in} \tag{1}$$

In a typical neuron, the concentration of sodium outside the cell (~460 mM) is much higher than the concentration of sodium inside the cell (~50 mM), while the concentration of potassium is much higher inside the cell (~400 mM) than outside the cell (~10 mM) [Nicholls et al., 1992]. These differences in concentration, and the relatively low permeability of the membrane give rise to a resting potential across the membrane of ~ -80 mV, measured from the inside with respect to the outside.

Within the cell membrane are a number of integral proteins, including intracellular and extracellular receptors, as well as a number of membrane-spanning proteins that make up pores through the membrane that allow the passage of ions through the membrane (conduct ionic current). These proteins are modeled by electrical resistors or conductors (Fig. 2A), and in many cases are non-linear with the conductance varying as a function of the transmembrane voltage.

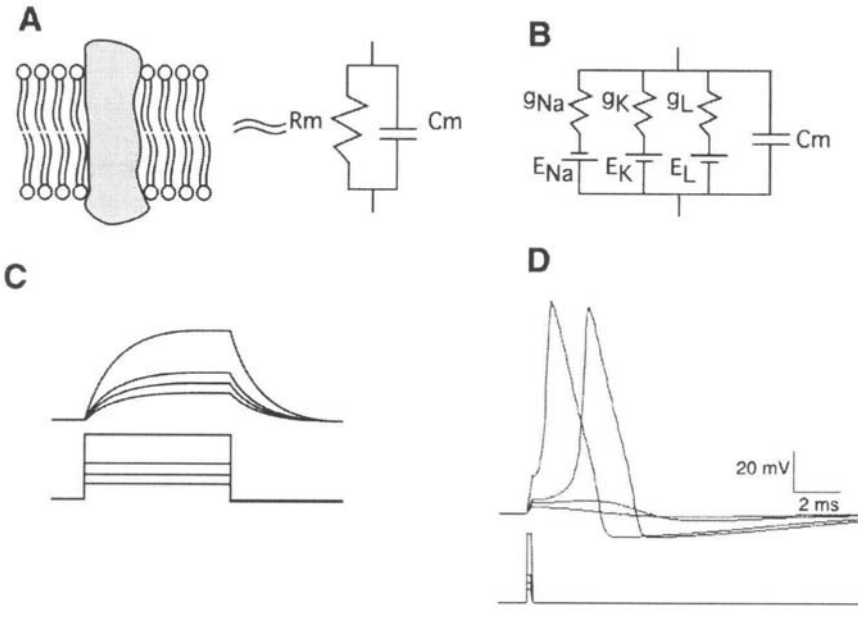

Fig. 2. Models of the nerve fiber membrane. **(A)** A patch of membrane can be modeled as a parallel resistor-capacitor circuit where the capacitor (C_m) represents the lipid bilayer and the resistor (R_m) represents the transmembrane proteins that constitute the ion channels. **(B)** Non-linear model of the nerve fiber membrane incorporating non-linear sodium (g_{Na}) and potassium (g_K) conductances, a linear leak conductance (g_L), and batteries for the sodium (E_{Na}), potassium (E_K), and leak (E_L) Nernst potentials. **(C)** Response of a linear model of the nerve membrane to current pulses injected intracellularly. Top traces are transmembrane potential measured inside with respect to outside and bottom traces are the injected current pulses. **(D)** Response of the non-linear model of the nerve membrane to current pulses injected intracellularly. Top traces are transmembrane potential measured inside with respect to outside and bottom traces are the injected current pulses.

The first order model of a patch of neuronal membrane is a parallel resistor-capacitor circuit (Fig. 2A). Applying Kirchoff's Current Law to this circuit yield a first-order differential equation describing the changes in voltage across the membrane, where C_m is the membrane capacitance and R_m is the membrane resistance, $V_i(t)$ is the voltage at the inside of membrane and $V_o(t)$ is the voltage at the outside of the membrane:

$$C_m \frac{d[V_i(t)-V_o(t)]}{dt} + \frac{[V_i(t)-V_o(t)]}{R_m} = 0 \qquad (2)$$

Defining the reduced transmembrane voltage $V_m=V_i-V_o$ results in an equation that describes the changes in transmembrane voltage from the rest potential, with the polarity defined as the voltage inside with respect to the voltage outside:

$$Cm\frac{dV_m(t)}{dt}+\frac{V_m(t)}{R_m}=0 \tag{3}$$

The response of this model to current stimuli injected intracellularly is shown in Fig. 2C. When an intracellular source, I_{in}, is turned on at time zero it results in an exponential change in transmembrane potential given by the solution to the differential equation, where *u(t)* is the unit step function:

$$V_m(t)=I_{in}\cdot R_m\cdot[1-e^{-t/R_mC_m}]\cdot u(t) \tag{4}$$

3.2. Active model of a membrane patch

As described above, the conductances present in the neural membrane are non-linear, and as shown in Fig. 2D the linear model derived above is unable to account for the response of an neuron to current stimuli injected intracellularly. At smaller injected current amplitudes, the behavior of the non-linear model is well approximated by the linear model. However, at current amplitudes larger than threshold, defined as the minimum current to generate an action potential, the linear model fails. Thus, the model needs to be modified. The revised model including non-linear sodium and potassium conductances that depend on the transmembrane voltage, a linear leakage conductance, a membrane capacitance, and batteries in series with the membrane conductances to represent the transmembrane voltage due to differences in ionic concentrations inside and outside the cell (Nernst potentials, Eq. 1) is shown in Fig. 2B[10]. Application of Kirchoff's current law yields the first-order non-linear differential equation describing the transmembrane potential:

$$Cm\frac{dV_m(t)}{dt}+I_{Na}(V_m,t)+I_K(V_m,t)+I_L(V_m,t)=0 \tag{5}$$

The magnitude of each ionic current depends on the value of that ionic conductance, as well as the difference between the transmembrane voltage and the reversal (Nernst) potential for that ion, where E_{ion} is the Nernst potential for each ion (see Eq. 1):

$$I_{ion}(Vm,t)=g_{ion}(V_m)\cdot(V_m(t)-E_{ion}) \tag{6}$$

and Eq. 5 becomes

$$Cm\frac{dV_m(t)}{dt} + g_{Na}(V_m)\cdot(V_m(t)-E_{Na}) + g_K(V_m)\cdot(V_m(t)-E_K) + g_L(V_m(t)-E_L) = 0 \tag{7}$$

The conductance for each ion is described by the product of the maximum conductance (equal to ionic conductance if all channels were open) for that ion multiplied by a gating factor or factors, which take values between 0 and 1. The potassium conductance is described by the equation:

$$g_K = \bar{g}_K n^4 \tag{8}$$

where n is an activation variable, and the sodium conductance is described by the equation:

$$g_{Na} = \bar{g}_{Na} m^3 h \tag{9}$$

where m is an activation variable and h is an inactivation variable.

The time rate of change of the potassium conductance activation variable, n, is described by the first order differential equation:

$$\frac{dn}{dt} = \alpha_n(1-n) - \beta_n n \tag{10}$$

where (1-n) can be thought of as the proportion of potassium channels not in the activated state (closed) and n can be thought of as the proportion of potassium channels in the activated state (open). Analogous equations describe the rate of change of the sodium activation parameter, m, where m can be thought of as the proportion of sodium channels in the activated state (open) and the sodium inactivation parameter, h, where h can be thought of as the proportion of sodium channels not in the inactivated state (de-inactivated). The rate constants, α and β that describe the transitions between states are functions of membrane potential[10].

An alternate formulation to describe the ionic conductance activation and inactivation variable arises from the solution to the first-order differential equation (Eq. 10), and for the potassium channel is given by:

$$n(t) = n_\infty - (n_\infty - n_o)e^{(-t/\tau_n)} \tag{11}$$

where τ_n is the time constant for activation of the potassium channel (Fig. 3**B**) and is given by the equation:

$$\tau_n = \frac{1}{\alpha_n + \beta_n} \tag{12}$$

where n_0 is the initial value of n, and n_∞ is the steady state value of n at a particular membrane potential (Fig. 3A). The steady-state values of the gating parameters the gating time constants depend on transmembrane voltage, since the rate constants α and β are functions of transmembrane voltage.

The above description of the non-linear model of a patch of neuronal membrane is based upon the properties of the squid giant axon. While nerve fibers and other neurons in other species have different ionic conductances, the underlying mathematical descriptions of these ionic conductances can be formulated in an analogous manner. The properties of myelinated axons were first quantified in frog[3]. Later experiments in mammalian myelinated nerve fibers demonstrated that the potassium conductance at the nodes of Ranvier is very small[1], and the impact of model selection on excitation properties was considered by Rattay and Aberham[17]. In many cases potassium conductances are ignored and the fine structure of the fiber is not considered. However, the human myelinated nerve fiber contains a wealth of ionic conductances, and accurate representation of these conductances, as well as the fiber geometry and myelin sheath[18] are required to reproduce the excitation properties of human nerve fibers[12]. Further, when considering the properties of neuronal cell bodies and dendrites, a large variety of voltage dependent sodium, potassium, and calcium conductances must be considered, as well as calcium-dependent potassium conductances, as well as ligand-gated ionic conductances[9]. Finally, the above description is deterministic, while actual ion channels have stochastic properties. The deterministic model treats all individual channels as one channel with a large maximum conductance, and the stochastic properties of ion channels can influence threshold, latency, and firing properties of neurons[14,21].

4. Reconstruction of the Action Potential

The first-order non-linear differential equation describing the transmembrane voltage can be solved to reconstruct the response of a membrane patch to an intracellular current pulse. An example of this for sub-threshold, threshold, and supra-threshold stimuli is shown in Fig. 2D. One advantage of the mathematical model is that the behavior of the individual currents and conductances can be examined to understand their roles in generation of the action potential (Fig. 3).

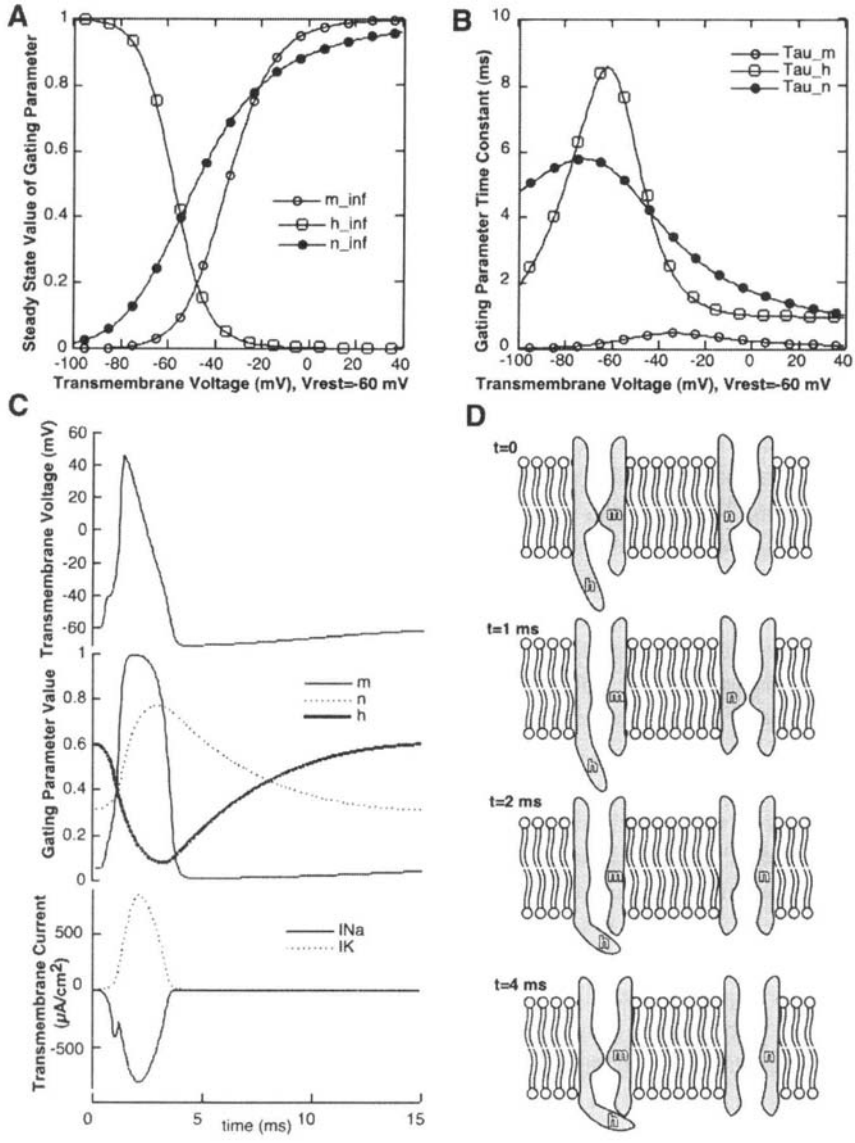

Fig. 3. Parameters of the Hodgkin-Huxley model of a patch a nerve membrane. **(A)** Steady-state values of the sodium conductance activation parameter (*m_inf*), sodium conductance inactivation parameter (*h_inf*), and potassium conductance activation parameter (*n_inf*) as a function of transmembrane voltage. **(B)** Values of the time constants for the sodium conductance activation parameter (*Tau_m*), the sodium conductance inactivation parameter (*Tau_h*), and the potassium conductance activation parameter (*Tau_n*) as a function of transmembrane voltage. **(C)** Reconstruction of the action potential. Transmembrane potential (measured inside with respect to outside), the conductance gating parameters, and the ionic currents (inward current is negative) during an action potential generated in response to an intracellular current pulse. **(D)** Cartoons of the conformation of representative sodium and potassium channels during the action potential. Times are referenced to panel C.

At rest, the sodium channels are in the closed-deinactivate state, and the potassium channels are in the closed state (Fig. 3D). This can be seen by examining the steady state values of each of the conductance gating parameters in Fig. 3A. Membrane depolarization, generated by outward flow of the intracellularly injected current, causes activation of the sodium channels and influx of sodium ions down their concentration gradient (recall that the concentration of sodium is much higher outside the cell than inside the cell). The larger the depolarization, the greater the increase in sodium conductance, and the larger the influx of sodium ions. If the degree of depolarization is sufficient, the sodium influx becomes regenerative—that is, the influx of positively charged sodium ions leads to further membrane depolarization, which leads to an increase in the sodium conductance, which leads to additional influx of sodium ions.

This process continues leading to a large change in transmembrane potential and the upstroke of the action potential (Figs. 3C, 3D at 1 ms). The process of sodium channel inactivation occurs in parallel with the activation of the sodium channels upon membrane depolarization. However, the time constant for sodium channel inactivation, τ_h, is an order of magnitude longer than the time constant for the process of sodium channel activation, τ_m (Fig. 3B). Thus, sodium channel inactivation lags sodium channel activation, and it is only after the upstroke of the action potential is complete that there is significant inactivation of the sodium channel. As the action potential approaches its peak, the transmembrane voltage approaches the sodium reversal potential, and the driving force for flux of sodium ions is reduced (Eq. 1). This results in the small "hitch" in the sodium current seen in Fig. 3C. During the repolarizing phase of the action potential the driving force for sodium is increasing and the channels are still in an open state, but sodium channel inactivation prevents continued sodium ion influx during repolarization (Figs. 3C, 3D at 2 ms). Upon repolarization, the sodium channels close (m decreases) stopping sodium influx, and they slowly de-inactivate (h increases) (Fig. 3D at 4 ms), restoring the channels to their resting state.

In parallel with the voltage dependent changes in the sodium conductance and the sodium driving force, which together produce the sodium current, voltage dependent changes are also occurring in the potassium conductance and the potassium ion driving force. At rest the potassium channels are ~70 % closed, and the driving force for potassium is close to zero, as the resting transmembrane potential is approximately equal to the potassium reversal potential. As the membrane is depolarized during the upstroke of the action potential, the driving force for the potassium ions increases in parallel with a delayed increase in the potassium conductance (Fig. 3D). At the peak of depolarization the driving force for potassium is at its maximum and the conductance is approaching its maximum (Fig. 3D at 2 ms). Thus, potassium ions flow down their concentration gradient, moving positive charge from inside the cell to outside the cell, and lead to membrane repolarization. As the membrane repolarizes, the potassium channels close (Fig. 3D at 4 ms) and the driving force for potassium ions decreases, restoring both to their resting states.

Thus, the excitability of neurons results from the concentration gradients of ions between the intracellular and extracellular spaces and the voltage-dependent ionic conductances arising from the membrane spanning protein pores that constitute the ion channels.

5. Models of the Axon

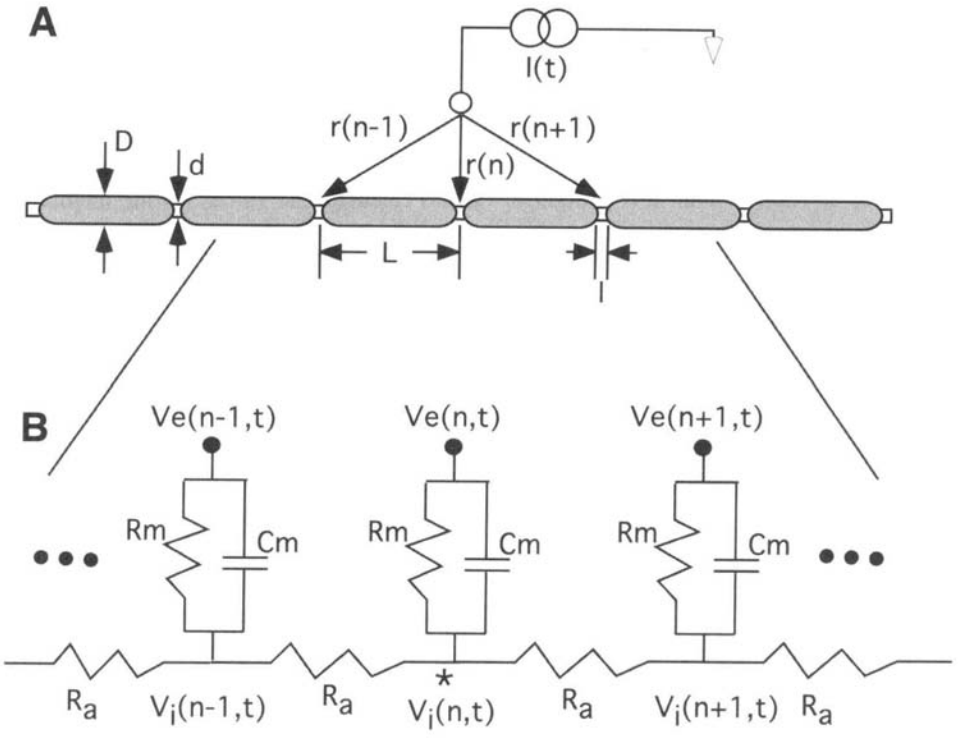

Fig. 4. Cable model of a myelinated nerve fiber. **(A)** Schematic representation of a myelinated nerve fiber in the presence of an extracellular stimulating electrode. **(B)** Electrical circuit equivalent of a section of a myelinated nerve fiber. In this simplified representation all membrane conductances are lumped into R_m.

In the previous section the properties of an individual patch of neuronal membrane were considered. Myelinated axons (Fig. 4) are composed of continuous tubes of membrane, surrounded at regular intervals by myelin sheaths (Schwann cells), and can be considered as a connection of individual patches of membrane. Each node of Ranvier can be modeled as a membrane patch. Adjacent nodes of Ranvier are separated by internodal spaces. If the myelin is assumed to be a perfect insulator, then the internode can be modeled as a tube of axoplasm and represented by an internodal resistance, R_a. We can calculate the internodal resistance as follows:

R_a = axoplasmic resistance
= axoplasmic resistivity*internodal length/cross sectional area of fiber
$= \rho_a * L/(\pi * d)$ (13)

In myelinated nerve fibers the internodal spacing (Fig. 4) is proportional to the fiber diameter (L=100*D) and the axon diameter, d, is proportional to the fiber diameter, D, (d=0.7*D). For a 10 μm diameter fiber (D=10 μm), with axoplasmic resistivity ρ_a=100 Ω-cm, the axoplasmic resistance is

$$R_a = 100\ \Omega\text{-cm} * 100 * 10 * 10^{-4}\ \text{cm} * 4/\pi * (0.7 * 10 * 10^{-4}\ \text{cm})^2 = 26\ \text{M}\Omega \quad (14)$$

The internodal resistances connect individual nodes of Ranvier that can be modeled as patches using the parallel RC circuit described above (Fig. 2A). If we cut and "unroll" each node of Ranvier then it is straightforward to calculate the values for the membrane resistance and membrane capacitance:

R_m = membrane resistance = specific membrane resistance/area of node
$= 2000\ \Omega\text{-cm}^2/\pi$*node length * node diameter
$= 2000\ \Omega\text{-cm}^2/\pi * 1.5 * 10^{-4}\ \text{cm} * 0.7 * 10 * 10^{-4}\ \text{cm}$
$= 6063\ \text{M}\Omega$ (15)

C_m = membrane capacitance = specific membrane capacitance*area of node
$= 1\ \mu\text{F/cm}^2 * \pi * 1.5 * 10^{-4}\ \text{cm} * 0.7 * 10 * 10^{-4}\ \text{cm}$
$= 0.33\ \text{pF}$ (16)

We now seek to derive an expression for the transmembrane voltage at one node of the fiber, or equivalently, one compartment of the cable model[11]. We consider the changes in transmembrane potential produced by an electric field present outside the nerve fiber that sets up potentials at each node of Ranvier, $V_e(n)$. Writing Kirchoff's Current Law at node n yields:

$$\frac{[V_i(n-1,t)-V_i(n,t)]}{R_a}+\frac{[V_i(n+1,t)-V_i(n,t)]}{R_a}+\frac{[Ve(n,t)-V_i(n,t)]}{R_m}+Cm\frac{d[Ve(n,t)-V_i(n,t)]}{dt}=0 \quad (17)$$

We then apply definition of reduced transmembrane voltage Vm(n,t)=Vi-Ve:

$$\frac{[V_m(n-1,t)-2V_m(n,t)+V_m(n+1,t)]}{R_a}+\frac{[V_e(n-1,t)-V_e(n,t)+V_e(n+1,t)]}{R_a}-\frac{V_m(n,t)}{R_m}-Cm\frac{d[V_m(n,t)]}{dt}=0 \quad (18)$$

re-arranging with source term on the right side yields:

$$Cm\frac{d[V_m(n,t)]}{dt}+\frac{V_m(n,t)}{R_m}-\frac{[V_m(n-1,t)-2V_m(n,t)+V_m(n+1,t)]}{R_a}=\frac{[V_e(n-1,t)-V_e(n,t)+V_e(n+1,t)]}{R_a} \quad (19)$$

This is called the cable equation and describes the changes in transmembrane potential generated in a nerve fiber by a set of extracellular potentials.

An example of the response of myelinated nerve fibers to extracellular stimulation, computed using Eq. 19, is shown in Fig. 5. The extracellular potentials generated at each node of Ranvier of a 10 μm and a 20 μm diameter nerve fiber by a point source electrode (Fig. 5**A**) were calculated using $V(r)=I\rho/4\pi r$, where I is the stimulating current, ρ is the resistivity of the extracellular medium, and r is the electrode to node distance. The maximum potential is the same in both fibers, but the change in potential between nodes is much larger in the 20 μm fiber, as the nodes are further apart (recall L=100*D). This is seen more clearly in Fig. 5**B**, which illustrates the magnitude of the second difference of the extracellular potentials along each of the fibers. The second difference of the extracellular potentials is the source term that drives membrane polarization (i.e., right hand side of Eq. 19)[16,20]. The magnitudes of the second differences are normalized by dividing by the peak value for the 20 μm fiber to illustrate that the source term is larger for the 20 μm diameter nerve fiber. Also note the triphasic shape of the second difference of the extracellular potential, as compared to the monotonic shape of the extracellular potentials (Fig. 5**A**). The larger source term for the 20 μm diameter nerve fiber dives rise to larger changes in transmembrane potential (Fig. 5**C**). The transmembrane potentials were normalized by dividing by the peak value in the 20 μm fiber to illustrate the difference between the two diameters. Note that the nerve fiber is depolarized immediately beneath the electrode (this is where action potential initiation will occur), and hyperpolarized in regions lateral to the electrode (compare Fig. 7**A**).

6. Excitation Properties of Myelinated Axons

In the sections above we derived electrical circuit equivalents of peripheral nerve fibers. In this section we quantify the response of nerve fibers to extracellular stimulation and interpret the results using the models.

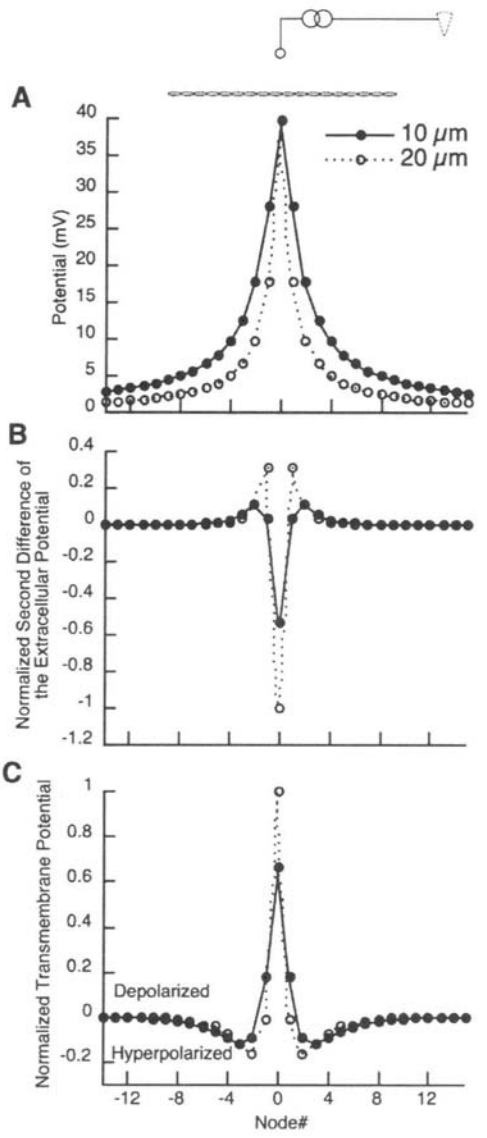

Fig. 5. The response of myelinated nerve fibers to extracellular stimulation. **(A)** Extracellular potentials at each node of Ranvier in 10 μm and 20 μm diameter nerve fibers from a point source electrode positioned 1mm above the central node of the fibers. The extracellular potential was calculated using $V(r)=Ip/4\pi r$, where I is the stimulating current (0.1 mA), ρ is the resistivity of the extracellular medium (500 Ω-cm), and r is the electrode to node distance. **(B)** Magnitude of the source term driving membrane polarization, i.e., the right hand side of Eq. 19, for the 10 μm and 20 μm fibers as a function of the node number. The magnitudes of the second difference of the extracellular potentials were normalized to the peak value for the 20 μm fiber to illustrate that the source term is smaller in the smaller diameter nerve fiber. **(C)** Profile of transmembrane potential generated in the 10 μm and 20 μm nerve fibers. Again, the transmembrane potentials were normalized to the peak value in the 20 μm fiber to illustrate the difference between the two diameters.

6.1. Strength-duration relationship

The threshold stimulus amplitude necessary for excitation, I_{th}, increases as the duration of the stimulus is decreased. The strength-duration relationship describes this phenomenon and is given by either the Lapique Equation (Eq. 20a) or the Weiss Equation (Eq. 20b), with the Weiss equation providing a better fit to most data[13], and an example of a strength-duration curve is shown in Fig. 6**A**.

$$I_{th} = \frac{I_{rh}}{1 - \exp^{(-PW/\ln(2)T_{ch})}} \tag{20a}$$

$$I_{th} = I_{rh}[1 + (T_{ch} / PW)] \tag{20b}$$

The parameter I_{rh} is the rheobase current, and is defined as the current amplitude necessary to excite the neuron with a pulse of infinite duration. The parameter T_{ch} is the chronaxie and is defined as the pulse duration necessary to excite the neuron with a pulse amplitude equal to twice the rheobase current.

6.2. *Charge-duration relationship*

The amount of charge necessary for excitation can be determined directly from the strength duration relationship. The resulting charge duration relationship is given by Eqs. 21a and 21b (for the Lapique and Weiss Formulations, respectively) and is shown in Fig. 6**B**.

$$Q_{th} = \frac{PW \cdot I_{rh}}{1 - \exp^{(-PW/\ln(2)T_{ch})}} \tag{21a}$$

$$Q_{th} = I_{rh}[PW + T_{ch}] \tag{21b}$$

The charge required for excitation decreases as the duration of the pulses decreases (Fig. 6**B**). Thus, although short pulses require higher currents for excitation, shorter pulses are more efficient at generating excitation than are longer pulses. Reducing the charge required for excitation reduces the probability of electrode corrosion or tissue damage and reduces stimulator power requirements. Shorter pulses also decrease the gain between the stimulus magnitude and the number of nerve fibers activated by increasing the threshold difference between different diameter nerve fibers[4]. Similarly, shorter

pulses increase the spatial selectivity of stimulation by increasing the threshold difference between nerve fibers lying at different distances from the electrode[6].

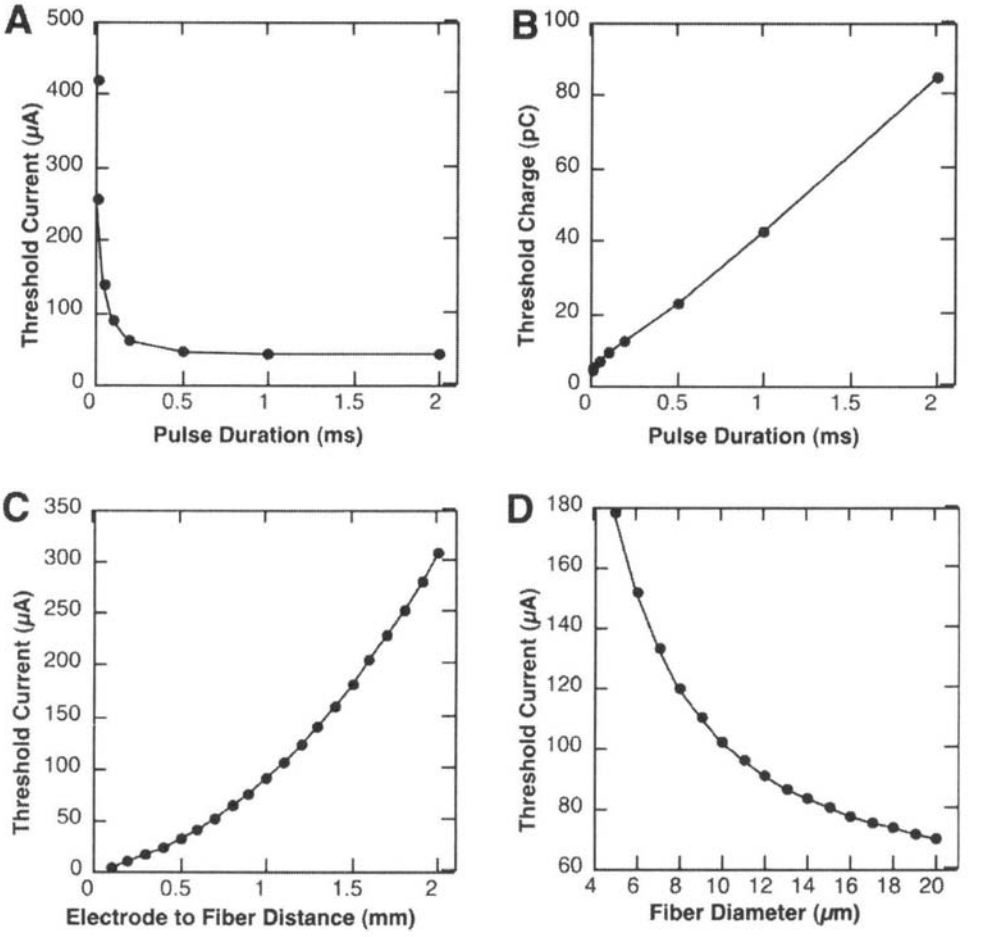

Fig. 6. Excitation properties of myelinated nerve fibers determined with a cable model. **(A)** The strength-duration curve describes the threshold current as a function of the stimulus duration. **(B)** The charge-duration curve describes the threshold charge as a function of the stimulus duration and is obtained by integration of the strength-duration relationship. **(C)** The current-distance curve describes the threshold current as a function of the electrode to nerve fiber distance. **(D)** The current-diameter curve describes the threshold current as a function of the nerve fiber diameter.

6.3. *Current-distance relationship*

The current required for extracellular stimulation of axons also depends on the spatial relationship between the electrode and the nerve fiber and the nerve fiber diameter[11]. Transmembrane potentials generated by extracellular current are largest in the fibers closest to the stimulating electrode, thus less current is required to stimulate neurons in the proximity of the electrode (Fig. 6C). As the distance between the electrode and the fiber increases, the threshold, I_{th}, increases, and for excitation of myelinated nerve fibers with a point source electrode this relationship is described by equation 22.

$$I_{th} = I_R + k \cdot R^2 \tag{22}$$

The offset, I_R, determines the absolute threshold and the slope, k, determines the threshold difference between fibers at different distances, R, from the electrode[19].

6.4. *Current-diameter relationship*

Similarly, in response to an externally applied stimulus, nerve fibers with a larger spacing between the nodes of Ranvier experience transmembrane potential changes that are larger than those in fibers with a smaller internodal spacing[11]. Under normal conditions the larger diameter nerve fibers have larger internodal spacings. Thus, larger diameters fibers are activated at smaller stimulus amplitudes than the smaller diameter fibers. The current-diameter relationship is given by Eq. 23 and is shown in Fig. 6**D**.

$$I_{th}(D) = I_D + \frac{a}{\sqrt{D}} \tag{23}$$

The observation that threshold is inversely related to the fiber diameter can be understood by examination of the cable equation describing changes in transmembrane potential in response to an extracellular electric field. There are two contributions to the source term on the right hand side of Eq. 19 — the second difference of the extracellular potential and 1/Ra:

$$\frac{[V_e(n-1,t) - V_e(n,t) + V_e(n+1,t)]}{R_a} \tag{24}$$

Since the internodal distance is proportional to the fiber diameter (L=100D) both of these terms are larger in larger diameter nerve fibers. For the same extracellular field, the second difference of the extracellular potential is dependent on the internodal spacing.

Since the internodal spacing is larger for larger diameter nerve fibers (L=100D), the differences between the potentials at nodes, n-1, n, and n+1 will be larger, the source term will be larger (Fig. 5B) and the threshold will be lower. From Eq. 13. Ra = axoplasmic resistivity*internodal length/cross sectional area of fiber which means that Ra $\propto D/D^2=1/D$. Thus, as D increases, Ra decreases and the source term increases. Thus the source term is larger and the threshold for larger diameter nerve fibers is lower than the threshold for smaller diameter nerve fibers.

6.5. Conduction velocity

The velocity at which action potentials travel along myelinated nerve fibers is proportional to the fiber diameter (CV=6 m/s/μm). This relationship arises from the correlation between fiber diameter and internodal spacing (L=100D). Since larger diameter fibers have larger internodal spacing, the action potential travels further as it moves from node to node (salutatory conduction) in large diameter fibers than it does in small diameter fibers.

6.6. *Stimulus polarity*

The threshold for excitation is dependent on the polarity of the pulse. During stimulation with a cathodic current (i.e., electrode is a current sink), the membrane nearest to the electrode is depolarized by outward current flow, and an action potential is generated (Fig. 5C). However, during stimulation with an anode (i.e., electrode is a current source), the membrane nearest the electrode is hyperpolarized by inward current flow (Fig. 7A). There are two ways in which membrane hyperpolarization can lead to neuronal excitation: virtual cathodes and anode break excitation.

Virtual cathodes arise from the triphasic form of the transmembrane potential generated by stimulation. While the part of the fiber immediately under the electrode is hyperpolarized by inward current flow, this region of hyperpolarization is surrounded by two flanking regions of depolarization arising from outward current flow (arrows in Fig. 7A) that are referred to as "virtual" cathodes. Action potential initiation (excitation) may take place at the virtual cathodes if the applied anodal current is sufficient to bring the depolarized portion of the membrane to threshold. Typically, current thresholds for excitation with an anodal current, via virtual cathodes, are 5–8 times larger than the threshold current for direct cathodal stimulation (Fig. 5C).

Anode break excitation arises from the voltage-dependent properties of the sodium conductance (Fig. 7B). During membrane hyperpolarization, the sodium channels are de-inactivated (h is increased) and de-activated (m is decreased). Following termination of the pulse and the release of hyperpolarization, the membrane potential recovers toward the rest potential. Due to the slow time constant of h (Fig. 3B), the sodium channels

remain in a de-inactivated state, while the level of activation, m, recovers toward its resting value. This puts the membrane in a hyper-excitable state, as compared to rest, and if h was sufficiently elevated by the hyperpolarization, the influx of sodium during the return of membrane potential toward rest can result in generation of an action potential. Since this excitation occurs at the termination of the current pulse, it is referred to as "break" excitation. Since the time constant of h is quite long (Fig. 3**B**), anode break excitation generally requires long duration hyperpolarizing pulses.

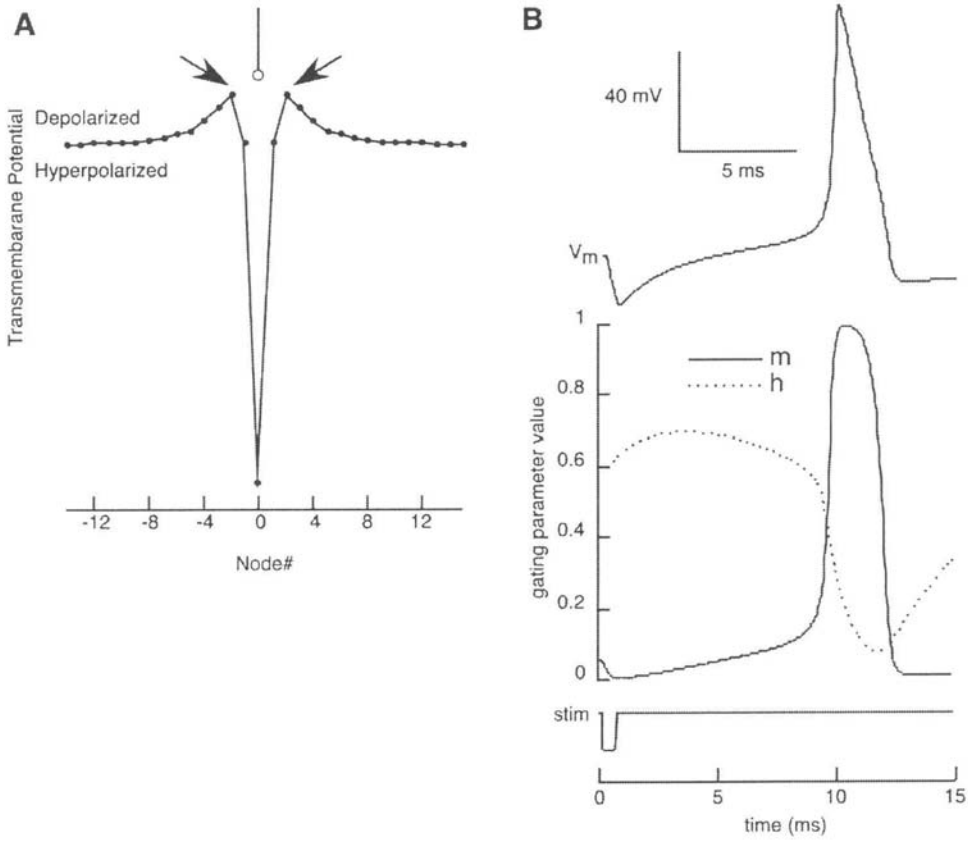

Fig. 7. Excitation of myelinated nerve fibers with anodic stimuli. (**A**) Profile of transmembrane potential generated in a myelinated nerve fiber by an extracellular anodic electrode. The nerve fiber is hyperpolarized immediately under the electrode and depolarized at the flanking nodes by the virtual cathodes (arrows). (**B**) Transient hyperpolarization results in anode break excitation. Transmembrane potential (measured inside with respect to outside), the conductance gating parameters, and the stimulus pulse during an action potential generated upon release of a 500 μs anodic current pulse.

6.7. Refractory period

Following the generation of an action potential there is a short period when larger currents are required to generate a second action potential. This phenomenon is referred to as the refractory period and is illustrated in Fig. 8. In Fig. 8**A** a second stimulus pulse applied 5 ms after the first stimulus pulse does not generate a second action potential. However, when the same stimulus is applied 10 ms after the first stimulus a second action potential is generated. The origin of the refractory period can be explained with reference to the properties of the sodium conductance. When the second pulse is applied shortly after the first pulse (5 ms in Fig. 7**A**), the sodium channels are still in a state of inactivation ($h \approx 0.3$ as compared to its rest value of ≈ 0.6), and the membrane is hypo-excitable. However if sufficient time elapses after first pulse (10 ms in Fig. 7**B**), the sodium channels recover from inactivation ($h \approx 0.55$ as compared to its rest value of ≈ 0.6), and the membrane is able to generate a second pulse. Thus, the slow time course of the recovery of voltage-dependent sodium channels from inactivation (Fig. 3**B**) gives rise to a transient reduction in excitability called the refractory period.

7. Conclusions

Electrical activation of the nervous system is a powerful means to study physiological mechanisms and a technique to restore function to persons with neurological disorders. Quantitative models provide a means to understand the non-linear properties of the neuronal membrane, as well as the response of nerve fibers to extracellular stimulation. The excitation phenomena described in this chapter, while appearing at the outset to be empirical observations, could all be explained by reference to the cable-description of myelinated nerve fibers and an understanding of the non-linear conductances that underlie neuronal excitability. Further, accurate quantitative models provide tools for understanding the origins of measured phenomena[12], as well as powerful design tools that can be used to engineer stimuli that produce a desired response[5,7].

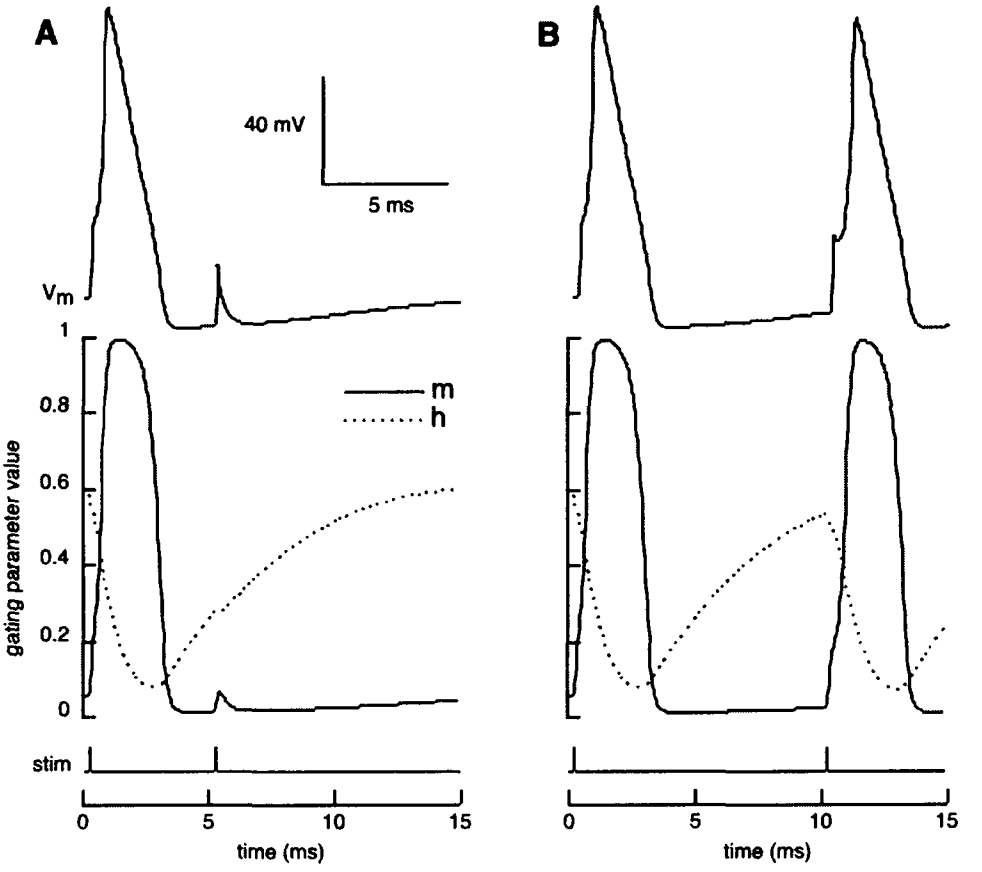

Fig. 8. Neurons exhibit an increase in threshold, called the refractory period, following generation of an action potential. Transmembrane potential (measured inside with respect to outside), the conductance gating parameters, and the stimulus pulses applied with either a 5 ms inter-stimulus interval (**A**) or a 10 ms inter-stimulus interval (**B**).

Acknowledgement

Preparation of this chapter was supported by National Institutes of Health Grants R21 NS43450 and R01 NS-40894.

References

[1] Chiu, S.Y., J.M. Ritchie, R.B. Rogart, D. Stagg. A quantitative description of membrane currents in rabbit myelinated nerve. *J. Physiology* 292:149-166, 1979.

[2] Crago, P.E. P.H. Peckham, J.T. Mortimer, J.P. Van Der Meulen. The choice of pulse duration for chronic electrical stimulation via surface, nerve, and intramuscular electrodes. *Annals of Biomedical Engineering* 2:252-264, 1974.

[3] Frankenhauser, B., A.F. Huxley. The action potential in the myelinated nerve fiber of xenopus laevis as computed on the basis of voltage clamp data. *J. Physiology* 171:302-315, 1964.

[4] Gorman, P.H., J.T. Mortimer. The effect of stimulus parameters on the recruitment characteristics of direct nerve stimulation. *IEEE Transactions on Biomedical Engineering* 30:407-414, 1983.

[5] Grill, W.M., J.T. Mortimer. Stimulus waveforms for selective neural stimulation. *IEEE Engineering in Medicine and Biology* 14:375-385, 1995.

[6] Grill, W.M., J.T. Mortimer. The effect of stimulus pulse duration on selectivity of neural stimulation. *IEEE Transactions on Biomedical Engineering* 43:161-166, 1996.

[7] Grill, W.M., J.T. Mortimer. Inversion of the current distance relationship by transient depolarization. *IEEE Transactions on Biomedical Engineering* 44:1-9, 1997.

[8] Grill, W.M., R.F. Kirsch. Neuroprosthetic applications of electrical stimulation. *Assistive Technology* 12:6-20, 2000.

[9] Hille, B. *Ion Channels of Excitable Membranes, 3rd Edition.* Sunderland: Sinauer Associates, 2001.

[10] Hodgkin, A.L., A.F. Huxley. A quantitative description of membrane current and its application to conduction and excitation in nerve. *J. Physiol.* 117:500-544, 1952.

[11] McNeal, D.R. Analysis of a model for excitation of myelinated nerve. *IEEE Transactions on Biomedical Engineering* 23:329-337, 1976.

[12] McIntyre, C.C., A.G. Richardson, W.M. Grill. Modeling the excitability of mammalian nerve fibers: influence of afterpotentials on the recovery cycle. *Journal of Neurophysiology* 87:995-1006, 2002.

[13] McIntyre, C.C., W.M. Grill. Sensitivity analysis of a model of mammalian neural membrane. *Biological Cybernetics* 79:29-37, 1998.

[14] Mino, H., W.M. Grill. Effects of stochastic sodium channels on extracellular excitation of myelinated nerve fibers. *IEEE Transactions on Biomedical Engineering* 49:527-532, 2002.

[15] Nicholls, J.G., A.R. Martin, B.G. Wallace. *From Neuron to Brain.* Sunderland: Sinauer Associates, 1992.

[16] Rattay, F. Analysis of models for extracellular fiber stimulation. *IEEE Transactions on Biomedical Engineering* 36:676-682, 1989.

[17] Rattay, F., M. Aberham. Modeling axon membranes for functional electrical stimulation. *IEEE Transactions on Biomedical Engineering* 40:1201-1209, 1993.

[18] Richardson, A.G., C.C. McIntyre, W.M. Grill. Modeling the effects of electric fields on nerve fibers: influence of the myelin sheath. *Medical and Biological Engineering and Computing* 38:438-446, 2000.

[19] Stoney, S.D., Jr., W.D. Thompson, H. Asanuma. Excitation of pyramidal tract cells by intracortical microstimulation: effective extent of stimulating current. *J.Neurophysiology* 31:659-669, 1968.

[20] Warman, E.N., W.M. Grill, D. Durand. Modeling the effects of electric fields on nerve fibers: determination of excitation thresholds. *IEEE Transactions on Biomedical Engineering* 39:1244-1254, 1992

[21] White, J.A., J.T. Rubinstein, A.R. Kay. Channel noise in neurons. *Trends in Neuroscience* 23:131-137, 2000.